Electronic structure, phonons and electron–phonon interaction in $MgXNi_3$ (X = B, C and N)

2006 J. Phys.: Condens. Matter 18 11089

(http://iopscience.iop.org/0953-8984/18/49/004)

INSTITUTE OF PHYSICS PUBLISHING JOURNAL OF PHYSICS: CONDENSED MATTER

J. Phys.: Condens. Matter **18** (2006) 11089–11101 doi:10.1088/0953-8984/18/49/004

Electronic structure, phonons and electron–phonon interaction in $MgXNi_3$ (X = B, C and N)

H M Tütüncü[1] **and G P Srivastava**

School of Physics, University of Exeter, Stocker Road, Exeter EX4 4QL, UK

Received 8 August 2006, in final form 7 November 2006
Published 22 November 2006
Online at stacks.iop.org/JPhysCM/18/11089

Abstract

Ab initio calculations have been performed to study the electronic structure, phonon dispersion relations, and the electron–phonon interaction for cubic superconductors $MgXNi_3$ with X = B, C and N. The electronic calculations are based upon the application of a plane wave basis, ultrasoft pseudopotentials, and the local density approximation of the density functional scheme. The electronic structure results are used, within the implementation of a linear response technique, for calculations of phonon states. Our calculations predict anomalous dispersion of the transverse acoustic branch along [111] in $MgCNi_3$, and of all the three acoustic branches in a larger region of the Brillouin zone for $MgNNi_3$. An explanation for the differences in the phonon dispersion and electron–phonon coupling parameter between these three materials has been put forward.

1. Introduction

In recent years, considerable effort has been spent on investigating ground state properties of $MgCNi_3$ because of a recent discovery of superconductivity in this material [1]. $MgCNi_3$ has the typical $SrTiO_3$ cubic perovskite structure, but with the oxygen atoms on the faces replaced by Ni atoms, and the Sr and Ti atoms replaced by Mg and C respectively, i.e. each C atom is surrounded by six Ni atoms. Due to the high concentration of Ni atoms, $MgCNi_3$ is expected to acquire a ferromagnetic ground state rather than a superconducting one. Indeed, it has been suggested that this material is a superconductor near the ferromagnetic quantum critical point [2]. Several experimental attempts [3–10] have been made to determine superconducting parameters of this intermetallic perovskite superconductor. Experimental results [7, 8] for the specific heat $C(T, H)$ appear to be consistent with the conventional Bardeen–Cooper–Schrieffer (BCS) behaviour. Additionally, experimental works [4, 5] have shown that the BCS electron–phonon interaction mechanism can be used to explain the transition temperature (T_c). A more recent experimental investigation [8] of the specific heat suggests that this material is

[1] Permanent address: Sakarya Üniversitesi, Fen-Edebiyat Fakültesi, Fizik Bölümü, Mithatpaşa, 54100 Adapazarı, Turkey.

characterized by a strong coupling, rather than the BCS weak coupling. This scenario requires more than one electronic crossing of the Fermi surface.

The above discussion suggests that a careful description of the band structure of $MgCNi_3$ is important. If there is a sharp peak close to the Fermi energy E_F, strong electron–phonon coupling can be expected. Photoemission and x-ray absorption measurements [11] have been made to measure the electronic structure of $MgCNi_3$. These experimental studies clearly show that there is a peak in the electronic density of states of $MgCNi_3$ which lies 0.1 eV below the Fermi level. Several theoretical methods have been used to investigate the electronic properties of $MgXNi_3$ (X = B, C, and N). These include the self-consistent tight-binding linear muffin tin orbital (TB-LMTO) method [12], the linear muffin tin orbital (LMTO) method [13, 14] and using density functional theory within the local density approximation [15–17]. Results from these works have indicated that the sharp peak just below the Fermi level is dominant in the electronic structure of $MgCNi_3$.

Inelastic neutron scattering measurements [18] have clearly indicated a softening of low frequency Ni modes in $MgCNi_3$. However, this softening phenomenon is thought not to be directly linked to the superconducting state of the material [18]. Regardless of such a link, it is important firstly to establish whether there does exist a soft phonon mode in the material. The linearized muffin tin orbital (LMTO) method [19] and *ab initio* mixed-basis perturbation method [18] have been used to obtain the phonon spectrum of this material. However, there are some differences between these theoretical results [18, 19]. For example, the Mg phonon modes in the LMTO results [19] lie at higher frequencies than the corresponding phonon modes in the *ab initio* mixed-basis perturbation results [18]. Although the *ab initio* method [18] observed an unstable phonon mode behaviour for the transverse acoustic phonon frequency at the X zone edge, this observation has not been made in the LMTO work [19]. On the other hand, the results from the two theoretical methods [18, 19] agree with each other for the highest optical phonon mode. Very recently, the phonon properties of this material have been reported by using a lattice dynamical theory based on pairwise interactions under the framework of the rigid ion model (RIM) [20]. In contrast to the *ab initio* calculations [18], this work produced an unstable acoustic phonon mode at the R zone edge point. Thus, the behaviour of the lowest acoustic branch in the phonon spectrum of $MgCNi_3$ is unclear.

In this work we have carried out *ab initio* calculations of the electronic band structure, lattice dynamics, and electron–phonon interaction for the cubic superconductors $MgXNi_3$ (X = B, C, and N). The electronic structure is calculated by employing the plane wave pseudopotential method within the local density approximation of the density functional scheme. The phonon dispersion relations are obtained by employing the linear response approach, based on the *ab initio* pseudopotential method [21]. The results for $MgCNi_3$ are compared and contrasted with previously published results [18–20].

2. Details of calculations

Our calculations were performed using the density functional theory within the local density approximation (LDA). The Ceperley–Alder electron correlation scheme [22] was used in the form parametrized by Perdew and Zunger [23]. Ion–electron interactions were treated by using the ultrasoft pseudopotentials of Rappe *et al* [24]. The wavefunctions were expanded in a plane wave basis set with the kinetic energy cut-off of 60 Ryd for all $MgXNi_3$ structures. In order to determine the equilibrium lattice constant and electronic structure, we used 120 special **k** points in the irreducible Brillouin zone. Integration of functions in the momentum space up to the Fermi surface is done with a Gaussian smearing technique [25], with the smearing parameter of 0.02 Ryd. The equilibrium lattice constant, bulk modulus, and the pressure derivative of the

bulk modulus were determined by fitting the total energy data to the Murnaghan equation of state [26].

We calculated the phonon spectrum of the $MgXNi_3$ crystals by employing a linear response (LR) approach, based on the *ab initio* pseudopotential method and a computer code due to Baroni and co-workers [21]. For the phonon calculations, we performed Brillouin zone integration by using a set of 84 special **k** points. Dynamical matrices were computed on a $4 \times 4 \times 4$ phonon **q**-point mesh, and a Fourier interpolation was used to obtain phonon frequencies for any chosen **q** vector. The resulting phonon frequencies were tested and are found to be accurate to within 0.3 meV compared to direct calculations at a few symmetry points. Phonon density of states calculations were made by using the tetrahedron method.

We have also calculated the electron–phonon interaction parameter in $MgXNi_3$. When the electron energies around the Fermi level are linear in the range of phonon energies, the phonon linewidth is given by Fermi's 'golden rule' formula [27, 28]

$$\gamma_{\mathbf{q}j} = 2\pi\omega_{\mathbf{q}j} \sum_{\mathbf{k}nm} |g^{\mathbf{q}j}_{(\mathbf{k}+\mathbf{q})m;\mathbf{k}n}|^2 \delta(\varepsilon_{\mathbf{k}n} - \varepsilon_F)\delta(\varepsilon_{(\mathbf{k}+\mathbf{q})m} - \varepsilon_F), \tag{1}$$

where the Dirac delta functions express energy conservation conditions. The matrix element for electron–phonon interaction is [27, 28]

$$g^{\mathbf{q}j}_{(\mathbf{k}+\mathbf{q}),m;\mathbf{k}n} = \sqrt{\frac{\hbar}{2M\omega_{\mathbf{q}j}}} \langle \phi_{(\mathbf{k}+\mathbf{q})m} | \mathbf{e}_{\mathbf{q}j} \cdot \vec{\nabla} V^{\mathrm{SCF}}(\mathbf{q}) | \phi_{\mathbf{k}n} \rangle, \tag{2}$$

where M is atomic mass and $\vec{\nabla} V^{\mathrm{SCF}}(\mathbf{q})$ is the derivative of the self-consistent effective potential with respect to the atomic displacement caused by a phonon with wavevector **q**.

The electron–phonon coupling parameter involving a phonon $\mathbf{q}j$ can be expressed as [27, 28]

$$\lambda_{\mathbf{q}j} = \frac{\gamma_{\mathbf{q}j}}{\pi\hbar N(\varepsilon_F)\omega^2_{\mathbf{q}j}} \tag{3}$$

where $N(\varepsilon_F)$ is the electronic density of states per atom and per spin at the Fermi level.

The sum in equation (1) is performed using a dense mesh ($24 \times 24 \times 24$ Monkhorst–Pack mesh) of **k** points in the irreducible Brillouin zone of the simple cubic structure. The Dirac delta functions in this equation were replaced with a Gaussian function of width 0.02 Ryd. Our results are not very sensitive to the Gaussian width due to the large number of **k** points sampled (see also [28, 29]). A convergence test with respect to the number of **k** points was carried out for $MgCNi_3$. Then, we observed that the chosen sampling of the $24 \times 24 \times 24$ **k** mesh is totally adequate.

3. Results

3.1. Structural and electronic properties

The values determined here for the equilibrium lattice constant, bulk modulus, and the pressure derivative of the bulk modulus for the $MgXNi_3$ (X = B, C, N) crystals in the ABO_3-like cubic perovskite structure are presented in table 1. For $MgCNi_3$, the resulting lattice constant, $a = 3.75$ Å, and bulk modulus $B = 2.02$ Mbar agree well with previous theoretical calculations [16–18]. However, our calculated lattice constant for this material is about 1.5% lower than the experimental value [9] of 3.807 Å, but this is a usual feature of LDA calculations.

The work of Shim *et al* [14] has clarified that the correlation effects of the Ni 3d electrons are not so important, so that there is no need to perform an LDA + U calculation to examine the band structure of the $MgXNi_3$ materials. Our calculated LDA electronic band structures

Table 1. Structural parameters for $MgXNi_3$. The present results are compared with previous experimental and theoretical results.

$MgXNi_3$	a (Å)	B (Mbar)	B'
$MgCNi_3$	3.75	2.02	4.49
Experimental [9]	3.807		
Theory [18]	3.76		
Theory [16]	3.77	2.10	
Theory [17]		2.14	
$MgNNi_3$	3.73	2.05	4.40
$MgBNi_3$	3.78	1.72	2.30

of these materials along the high symmetry directions in the simple cubic Brillouin zone are displayed in figure 1. The electronic structure of $MgCNi_3$ shows the metallic nature of this material, with two bands crossing the Fermi level along the Γ–M, Γ–R and X–R symmetry directions. However, there is a clear separation between occupied and unoccupied energy bands along the R–M symmetry direction. The total density of electronic states in figure 2 shows that there is a peak at around 0.1 eV below the E_F, which is due to an extremely flat band around M along the Γ–M, X–M and R–M symmetry directions. In agreement with experimental results [11], we have found two more peaks in the density of states at energies −1.2 and −2.0 eV below the Fermi level. The former peak can be related to a flat band along the X–R and R–M symmetry directions, while the latter peak is dominated by a flat band along the [100] symmetry direction. The lowest peak close to −13 eV, not shown in figure 1, corresponds to C 2s states.

Our electronic structure results are quite different from the LMTO results presented by Ignatov *et al* [19]. Large differences are found in the energy location of bands within ±1.5 eV of the Fermi level at the zone centre as well as along the principal symmetry directions ΓX and ΓM. There are no reports by Ignatov *et al* [19] of electronic bands along the symmetry direction ΓR, which is most important for the consideration of electron–phonon interaction, as discussed in the next section. In contrast, our results for the electronic band structure and the density of states are in good agreement with the LMTO calculations by Dugdale and Jarlborg [13] and Shim *et al* [14], and the LAPW calculations by Singh *et al* [15].

In general, the electronic structure of $MgBNi_3$ is similar to that of $MgCNi_3$. However, some differences have been observed due to the differences in the electronic structure of the B and C atoms. For $MgBNi_3$, we have observed a flat conduction band at approximately 5 eV above the Fermi level along the Γ–X symmetry direction. This band produces a clear peak in the electronic density of states for $MgBNi_3$. The band close to E_F along the M–X direction is quite different from the electronic structure of $MgCNi_3$: it is more dispersive because the hybridization between the B 2p state and the Ni 3d is stronger than that between the C 2p state and the Ni 3d state. The highest occupied band in the band structure of $MgNNi_3$ lies below approximately 0.5 eV below E_F along the Γ–X direction. For all the three materials, there is a peak in the electronic density of states close to E_F.

3.2. Dynamical properties

As the crystal structure of $MgXNi_3$ materials belongs to the space group O_h^1 ($Pm\bar{3}m$) with five atoms per primitive cubic unit cell, there are a total of fifteen phonon branches. Due to symmetry, the distinct number of branches is reduced along the principal symmetry directions Γ–X and Γ–R. In accordance with the point group of the lattice, at the zone centre the optical

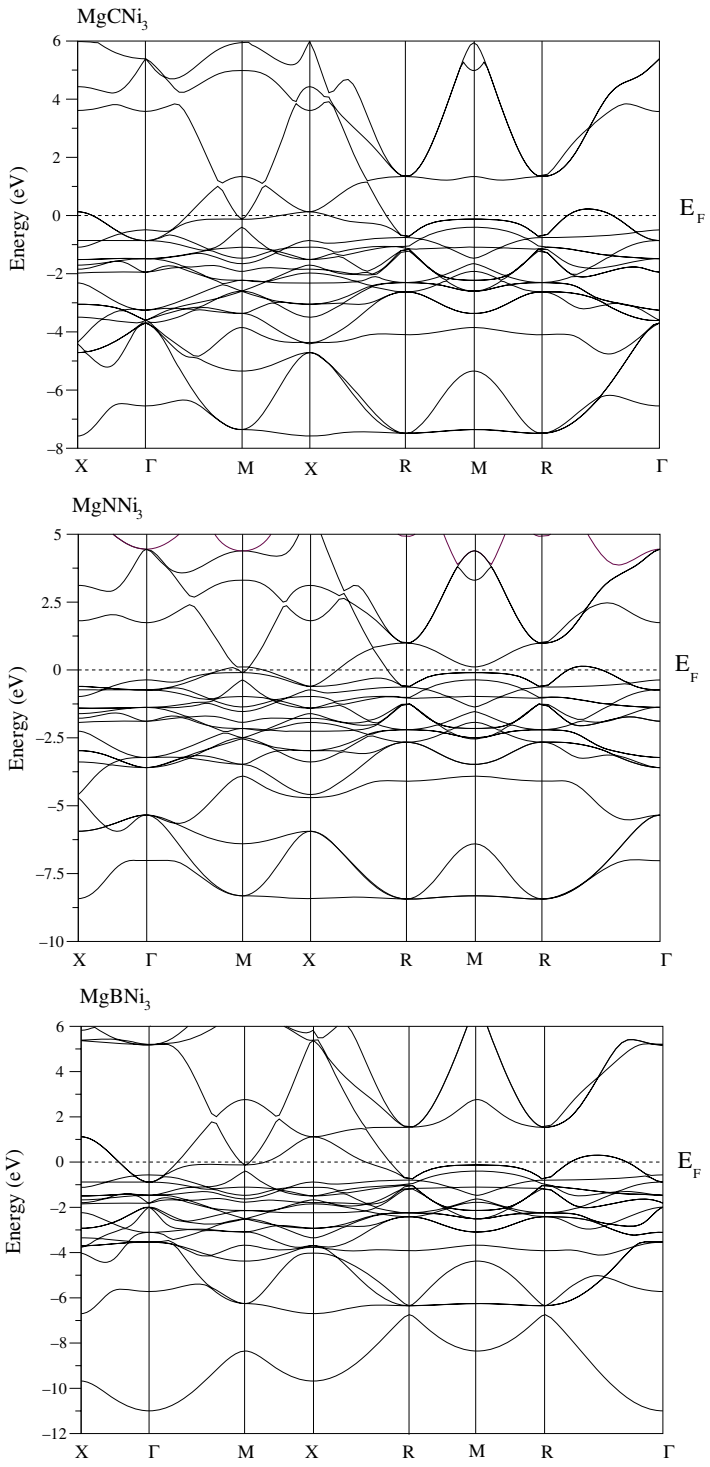

Figure 1. Calculated electronic band structure for $MgXNi_3$, where X = C, N and B. The Fermi level is set at 0 eV.

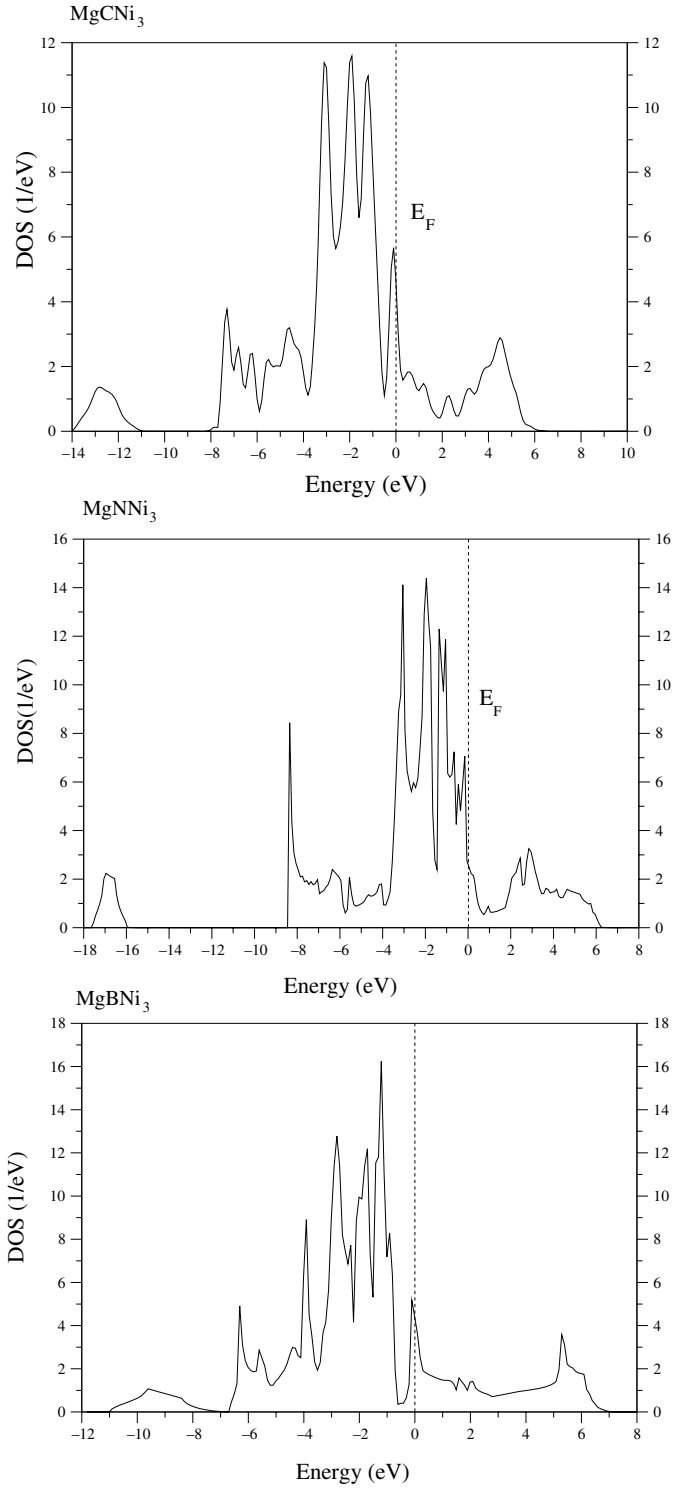

Figure 2. Calculated total electron density of states for $MgXNi_3$ where X = C, N and B. The Fermi level is set at 0 eV.

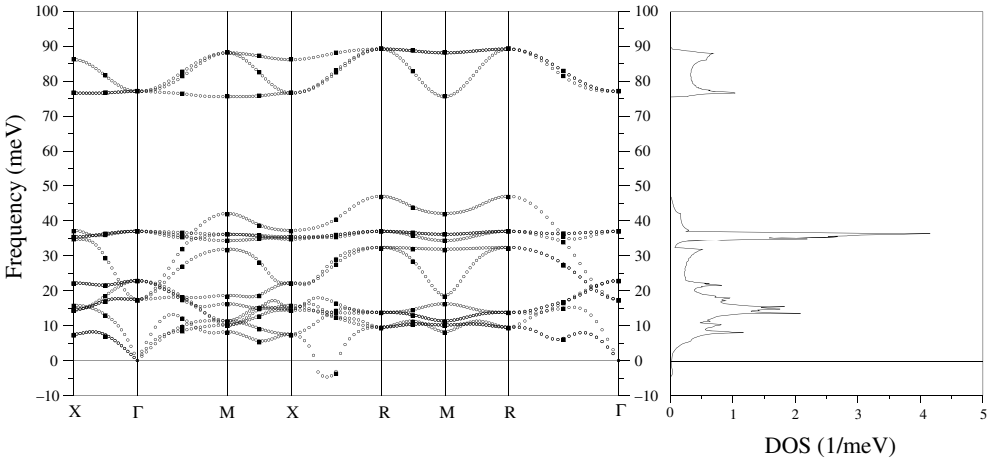

Figure 3. Phonon dispersion curves and the density of states for $MgCNi_3$. Open circles represent results calculated by Fourier interpolation while filled squares show the results from linear response calculations.

modes are triply degenerate and can be decomposed into four distinct classes. The four irreducible representations are $\Gamma(O_h^1) = F_{1u}^1 + F_{1u}^2 + F_{1u}^3 + F_{2u}$. None of these modes is Raman active.

3.2.1. Phonons and electron–phonon interaction in $MgCNi_3$. We present our calculated phonon dispersion results for $MgCNi_3$ in figure 3. The highest three optical branches are separated from the rest of the phonon branches. From the density of states, this gap is calculated to be 26 meV, which compares well with an experimental measurement of 23 meV [18]. The highest three branches result almost exclusively from vibrations of the C atom. The lowest of this group of branches is nearly flat along the Γ–M, Γ–X and M–X directions. The highest optical phonon branch along the main symmetry directions [100], [110] and [111] is found to be dispersive. Below the gap region, some of the optical branches are quite dispersive, except for one which is almost dispersionless at 36 meV. The flat branch originates from vibrations of Mg atoms. Due to lighter mass of C atoms, the three acoustic phonon branches originate from vibrations of Ni and Mg atoms. The peaks in the theoretical phonon density of states are at 8, 10, 15, 22, 33, 36, 78 and 89 meV. These results are in good agreement with the clearly resolved peaks at around 12, 16, 35, 80 meV in the neutron scattering measurements [18].

At the zone centre the four triply degenerate optical modes and their representations are: 22.88 meV (F_{2u}), 17.53 meV (F_{1u}^1), 37.03 meV (F_{1u}^2) and 77.11 meV (F_{1u}^3). The eigendisplacements of these phonon modes are shown in figure 4. The F_{2u} mode is characterized by vibrations of Ni atoms while the lowest F_{1u} mode involves atomic vibrations from all the five atoms in the unit cell. The other two F_{1u} modes are individually localized on Mg and C atoms. We have compared our calculated zone centre frequencies with previous RIM results [20] in table 2. As can be seen from this table, our results agree well with those given in the RIM work by Jha [20]. However, there is one serious difference between our results and the LMTO results [19] for the F_{1u}^2 mode: the LMTO work by Ignatov *et al* [19] places it at 48.00 meV, i.e. at around 10 meV higher than our and other theoretical results [18, 20].

Away from the zone centre, the phonon dispersion curves from our calculations show some notable differences from the theoretical results presented in [18–20]. As regards the dispersion of the highest three optical branches, in good agreement with the LMTO + LR results in [19]

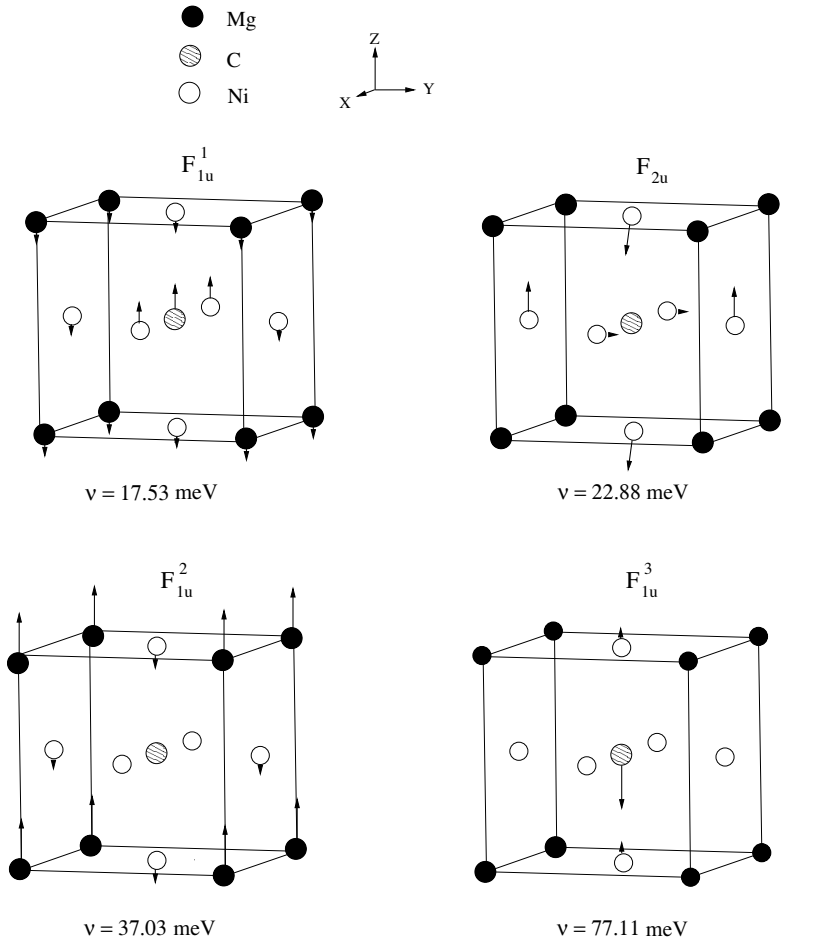

Figure 4. Eigenvector representations of zone centre optical phonon modes in $MgCNi_3$.

Table 2. Zone centre frequencies for $MgCNi_3$: comparison of the present results with the empirical RIM results.

Source	F^1_{1u}	F^2_{1u}	F^3_{1u}	F_{2u}
This work	17.53	37.03	77.11	22.88
RIM [20]	23.80	34.71	75.02	18.22

and the mixed-basis + LR results in [18], our results suggest that the empirical RIM results in [20] show wrong dispersion relations along the principal symmetry directions Γ–X and Γ–M. Most notably, our results for the lowest acoustic branch differ seriously from all of the three previous works in [18–20]. The LMTO + LR calculations in [19] show that this branch has a dip along Γ–X and Γ–R, and moreover is unstable along Γ–M. The mixed-basis + LR calculations in [18] predict an unstable branch along each of the principal directions Γ–X, Γ–M and Γ–R. The RIM calculations in [20] predict an unstable branch along Γ–M and Γ–R, but present no indication of any dip along Γ–X. In contrast to all these results, our work suggests

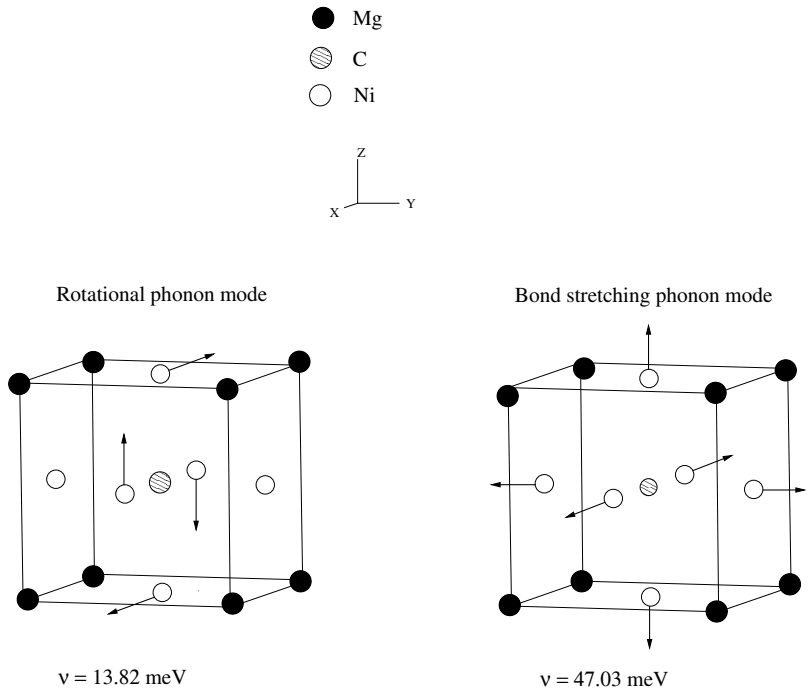

Figure 5. Eigenvector representations of the rotational and bond-stretching phonon modes at the R point in the Brillouin zone for $MgCNi_3$.

no dip in the dispersion of the lowest branch along Γ–X. We do obtain a shallow dip (i.e. an anomalous behaviour) along both Γ–M and Γ–R. Having found no evidence of any unstable phonon branch along the three principal symmetry directions in this cubic system, we searched along a few non-principal symmetry directions (such as M–X, X–R, R–M). We have found that a single acoustic branch becomes unstable in a small region midway between X–R. Previous theoretical calculations [18–20] have not presented results along this direction. Assuming that our results are beyond theoretical uncertainty, the resulting instability along X–R should be referred to as 'dynamic', as $MgCNi_3$ exists in a stable phase.

We establish the anomaly in the lowest acoustic branch as a dip at (0.275, 0.275, 0.275) in the [111] direction. At this **q** point, the electron–phonon coupling parameter for the lowest acoustic phonon mode is found to be $\lambda_{ac} = 1.54$. The frequency of this phonon mode is 5.90 meV, involving vibrations of Mg and Ni atoms. At the zone edge R, rotational and bond-stretching phonon modes have been identified with energies 13.82 and 47.03 meV. These modes are shown in figure 5. These modes are predicted at energies 13.00 and 43.30 meV in the previous theoretical work of Singh and Mazin [15], in agreement with our calculated values. Schematic representations of eleven vibrational phonon motions at the M point are presented in figure 6. In this figure, the electron–phonon coupling parameter for these eleven modes is also given. The largest electron–phonon coupling parameter $\lambda = 1.173$ has been obtained for the lowest acoustic phonon mode at 8.27 meV. In agreement with previous *ab initio* calculations [18], this phonon mode includes a rotational character due to opposing motion of Ni atoms. However, it appears to be a stable phonon mode in our calculations. The large values of λ discussed above are supported by the experimental investigations carried out by Wälte *et al* [10].

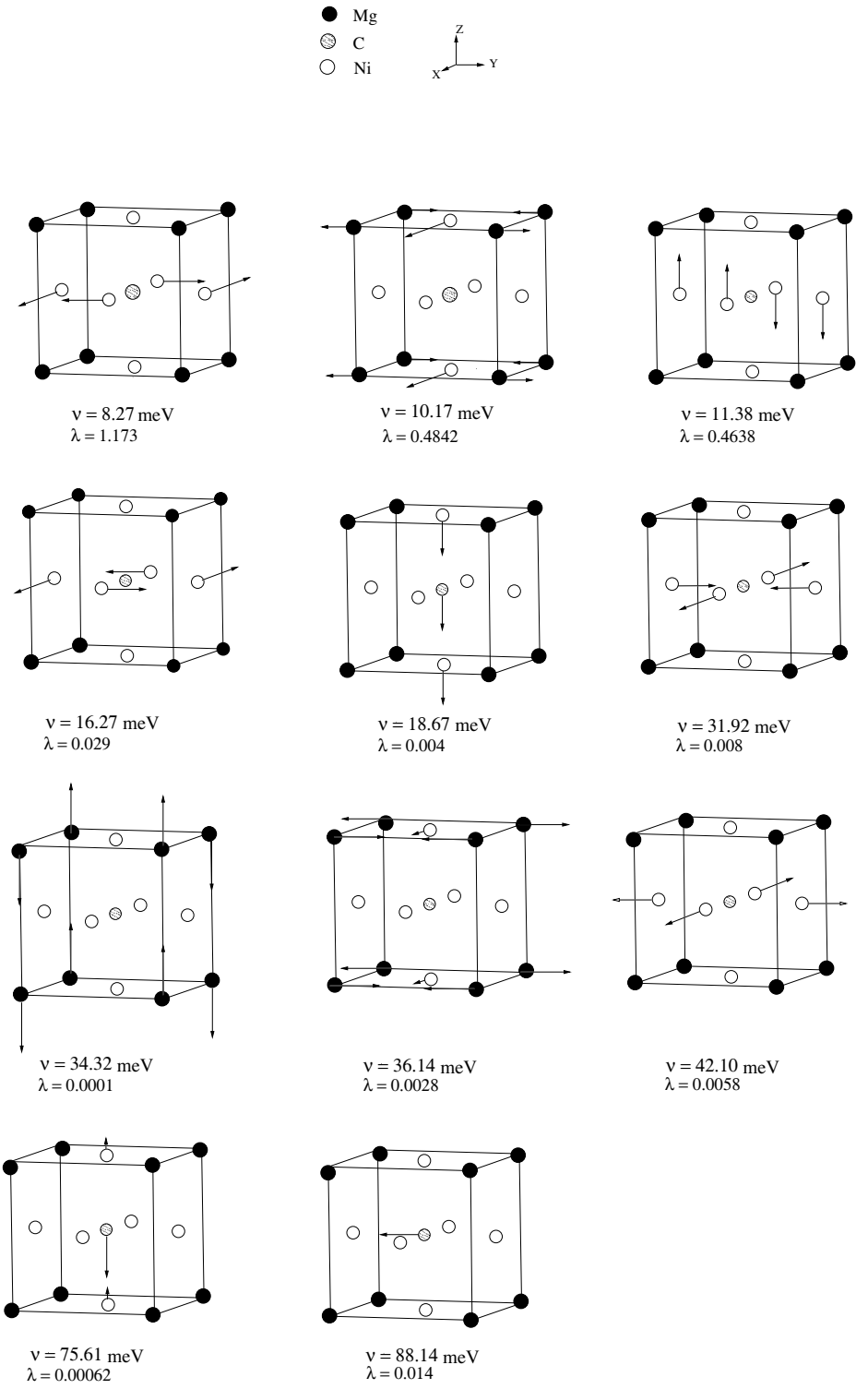

Figure 6. Eigenvector representations of M-point phonon modes in $MgCNi_3$.

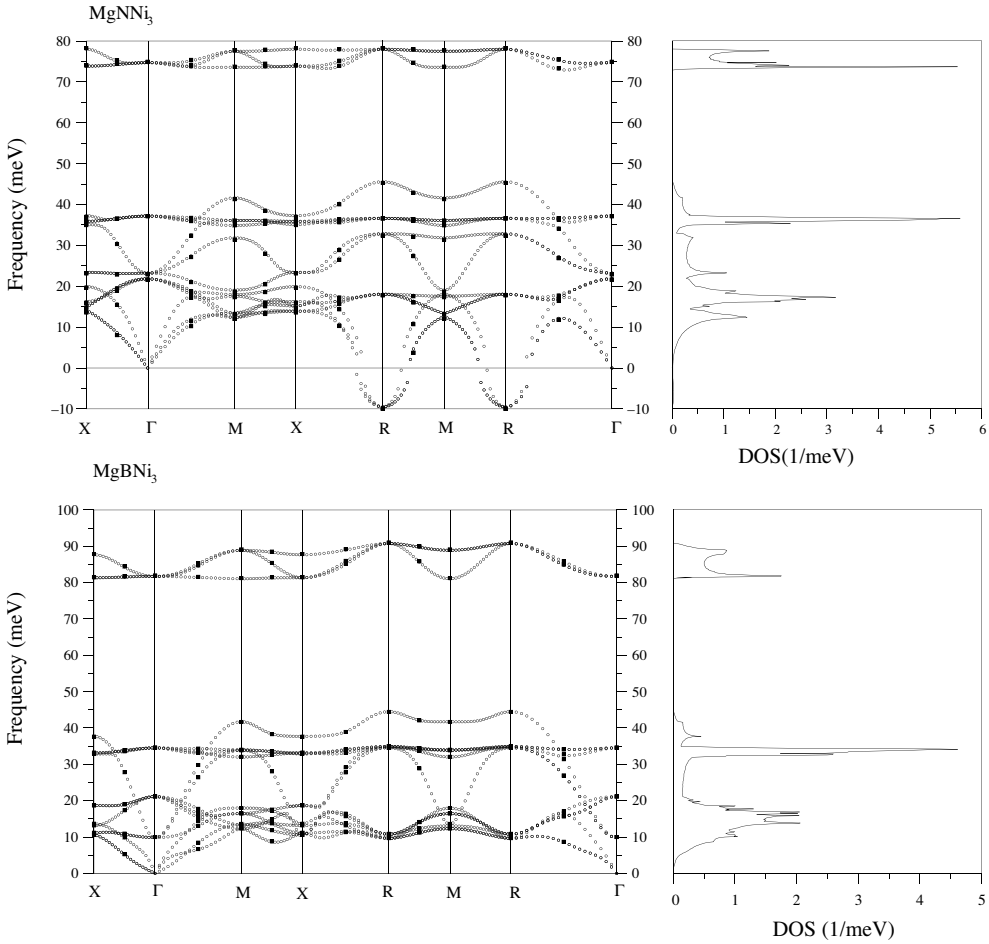

Figure 7. Phonon dispersion curves and the density of states for $MgNNi_3$ and $MgBNi_3$. Open circles represent results calculated by Fourier interpolation while filled squares show the results from linear response calculations.

3.2.2. Phonons and electron–phonon interaction in $MgBNi_3$ and $MgNNi_3$. The calculated phonon dispersion curves and density of states for $MgBNi_3$ and $MgNNi_3$ are displayed in figure 7. In contrast to the phonon spectrum of $MgCNi_3$, there is no anomalous behaviour in the transverse acoustic branch along the principal symmetry directions for these materials. However, the span of the region with unstable phonon modes increases across the sequence $MgBNi_3$, $MgCNi_3$, $MgNNi_3$. Since the masses of B, C and N atoms are very similar, this observation can be related to differences in the electronic structure and inter-atomic bonding in these materials. These changes are directly related to the gradual increase in the number of valence electrons: 35, 36 and 37 for these compounds, respectively. Our results clearly indicate that there are no unstable phonon modes in the phonon spectrum of $MgBNi_3$. For $MgCNi_3$, a single low frequency acoustic branch is found to be unstable in a small region along the X–R symmetry direction, but not along the principal symmetry directions [100], [110] and [111]. On the other hand, this instability is observed over a large area in the reciprocal space for $MgNNi_3$: unstable phonon modes are found along the Γ–R, X–R and M–R symmetry directions. For

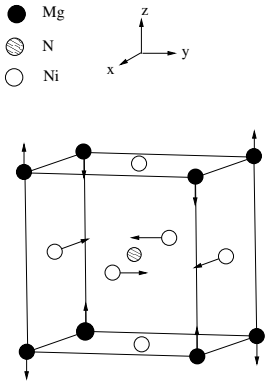

Figure 8. Eigenvector representations of the R-point unstable phonon mode in $MgNNi_3$.

the R point, the unstable phonon mode in $MgNNi_3$ is shown in figure 8. This phonon mode is triply degenerate and includes a rotational character of Ni atoms. Due to this rotational character, Ni d electrons and N p electrons can interact with each other strongly which leads to unstable phonon mode. This behaviour of the lowest phonon mode in $MgNNi_3$ suggests that this compound is structurally unstable in the cubic phase. At present this cannot be confirmed as there are no reports of any stable phases of this material.

Our calculations suggest that in general for all stable phonon modes the electron–phonon coupling parameter λ is higher for $MgCNi_3$ than for the other two materials. For example, at the zone edges X and M this parameter for the transverse acoustic mode has respective values 0.072 and 0.144 for $MgBNi_3$, and 0.193 and 0.320 for $MgNNi_3$. The corresponding values of 0.930 and 1.173 for $MgCNi_3$ are much higher. The strong electron–phonon coupling interaction in $MgCNi_3$ clearly indicates that this material can be described as a BCS-type superconductor.

4. Summary

We have presented results of *ab initio* calculations of the electronic structure, phonon dispersion relations, and electron–phonon interaction in cubic $MgXNi_3$ (X = B, C and N) by employing a plane wave basis set, ultrasoft pseudopotentials, and the local density approximation. The details of the electronic structure of $MgCNi_3$ are similar to those published in recent theoretical studies. However, results of our phonon calculations indicate a picture of normal and anomalous dispersion different to that presented in recent works on $MgCNi_3$. In particular, our work, in contrast to previous works, suggests that there is no dip in the dispersion of the lowest acoustic branch along the symmetry direction Γ–X. However, our work predicts a shallow dip in the dispersion of this branch along the other two principal symmetry directions, namely Γ–M and Γ–R. There are no anomalous phonon branches in $MgBNi_3$. In contrast, the lowest phonon branch in $MgNNi_3$ is characterized by instability over a large region in the reciprocal space, suggesting that this compound is structurally unstable in the cubic phase.

Acknowledgment

This work was carried out with financial support from EPSRC (UK).

References

[1] He T *et al* 2001 *Nature* **411** 54
[2] Blagoev K B, Engelbrecht J R and Bedell K S 1999 *Phys. Rev. Lett.* **82** 113
Wang Z, Mao W and Bedell K 2001 *Phys. Rev. Lett.* **87** 257001
Rosner H, Weht R, Johannes M D, Pickett W E and Tosatti E 2002 *Phys. Rev. Lett.* **88** 027001
[3] Singer P M, Imai T, He T, Hayward M A and Cava R J 2001 *Phys. Rev. Lett.* **87** 257601
[4] Li S Y, Fan R, Chen X H, Wang C H, Mo W Q, Ruan K Q, Xiong Y M, Luo X G, Zhang H T, Li L, Sun Z and Cao L Z 2001 *Phys. Rev.* B **64** 132505
[5] Shim J H, Kwon S K and Min B I 2001 *Phys. Rev.* B **64** 180510
[6] Kumary T G, Janaki J, Mani A, Jaya SM, Sastry V S, Hariharan Y, Radhakrishnan T S and Valsakumar M C 2002 *Phys. Rev.* B **66** 064510
[7] Lin J Y, Ho P L, Huang H L, Lin P H, Zhang Y L, Yu R C, Jin C Q and Yang H D 2003 *Phys. Rev.* B **67** 052501
[8] Mao Z Q, Rosario M M, Nelson K D, Wu K, Deac I G, Schiffer P, Liu Y, He T, Regan K A and Cava R J 2003 *Phys. Rev.* B **67** 094502
[9] Young D P, Moldovan M, Craig D D, Adams P W and Chan J Y 2003 *Phys. Rev.* B **68** 020501(R)
[10] Wälte A, Fuchs G, Müller K H, Handstein A, Nenkov K, Narozhnyi V N, Drechsler S L, Shulga S, Schultz L and Rosner H 2004 *Phys. Rev.* B **70** 174503
[11] Kim J H, Ahn J S, Kim J, Park M S, Lee S I, Choi E J and Oh S J 2002 *Phys. Rev.* B **66** 172507
[12] Szajek A 2001 *J. Phys.: Condens. Matter* **13** L595
[13] Dugdale S B and Jarlborg T 2001 *Phys. Rev.* B **64** 100508
[14] Shim J H, Kwon S K and Min B I 2001 *Phys. Rev.* B **64** 180510
[15] Singh D J and Mazin I I 2001 *Phys. Rev.* B **64** 140507
[16] Hase I 2004 *Phys. Rev.* B **70** 033105
[17] Johannes M D and Pickett W E 2004 *Phys. Rev.* B **70** 060507(R)
[18] Heid R, Renker B, Schober H, Adelmann P, Ernst D and Bohnen K P 2004 *Phys. Rev.* B **69** 092511
[19] Ignatov A Yu, Savrasov S Y and Tyson T A 2003 *Phys. Rev.* B **68** 220504
[20] Jha P K 2005 *Phys. Rev.* B **72** 214502
[21] Baroni S, de Gironcoli S, Dal Corso A and Giannozzi P 2001 *Rev. Mod. Phys.* **73** 515 and www.pwscf.org
[22] Ceperley D M and Alder B I 1980 *Phys. Rev. Lett.* **45** 566
[23] Perdew J P and Zunger A 1981 *Phys. Rev.* B **23** 5048
[24] Rappe A M, Rabe K M, Kaxiras E and Joannopoulos J D 1990 *Phys. Rev.* B **41** 1227
[25] Methfessel M and Paxton A T 1989 *Phys. Rev.* B **40** 3616
[26] Murnaghan F D 1944 *Proc. Natl Acad. Sci. USA* **50** 697
[27] Allen P B 1972 *Phys. Rev.* B **6** 2577
[28] Bauer R, Schmid A, Pavone P and Strauch D 1998 *Phys. Rev.* B **57** 1127
[29] Tse J S, Ma Y and Tütüncü H M 2005 *J. Phys.: Condens. Matter* **17** S991